The energy cost for flocking of active spins

Qiwei Yu[1, 2] and Yuhai Tu[1]

[1] *IBM T. J. Watson Research Center, Yorktown Heights, NY 10598*
[2] *Lewis-Sigler Institute for Integrative Genomics, Princeton University, Princeton, NJ 08544*

We study the energy cost of flocking in the active Ising model (AIM) and show that besides the energy cost for self-propelled motion, an additional energy dissipation is required to align spins in order to maintain the flocking order. We find that this additional alignment dissipation reaches its maximum at the flocking transition point in the form of a cusp with a discontinuous first derivative with respect to the control parameter. To understand this singular behavior, we analytically solve the two-site AIM model and obtain the exact dependence of the alignment dissipation on the flocking order parameter and control parameter, which explains the cusped dissipation maximum at the flocking transition. Our results reveal a trade-off between the energy cost of the system and its performance measured by the flocking speed and sensitivity to external perturbations. This trade-off relationship provides a new perspective for understanding the dynamics of natural flocks and designing optimal artificial flocking systems.

Understanding how collective coherent motion ("flocking") emerges from a system of self-propelled, interacting individuals has been a central question in nonequilibrium statistical physics and biophysics [1–3]. Familiar examples include birds, fish, bacteria [3, 4] and synthetic systems such as active colloids [5]. Theoretical studies have involved models of self-propelled, aligning particles with continuous [6–10] or discrete [11, 12] symmetry. Despite their diversity, these systems are all far from thermodynamic equilibrium [13] and thus a continuous dissipation of free energy is required to create and maintain the long-range flocking order. Indeed, energy dissipation plays a crucial role in driving living systems out of equilibrium to achieve important biological functions, such as adaptation [14], error correction [15–20], and temporal oscillation [21]. In this paper, we study the nonequilibrium thermodynamics of dry aligning active matter [22] aiming to elucidate the relationship between the energetic cost of flocking and its performance measured by the flocking speed and sensitivity.

The flocking dynamics can be studied at the microscopic level by prescribing the single-particle dynamics [6] or at the coarse-grained level with hydrodynamic field theories [7, 8]. In the latter case, irreversibility is measured by the information entropy production rate [23–25], but its connection to the heat dissipation rate is usually lost unless thermodynamic consistency is ensured, for instance, by relying on linear irreversible thermodynamics [26]. The energy dissipation also depends on coarse-graining [27–29], which makes it difficult to determine the true dissipation rate from coarse-grained field theories. Microscopic models, however, offer a more straightforward thermodynamic interpretation as energy dissipation (heat) can be determined directly from entropy production rate at the single-particle level.

Here, we investigate the energy dissipation of the active Ising model (AIM) [11, 12] which describes a lattice gas of Ising spins with ferromagnetic alignment and biased diffusion. The energy dissipation can be decomposed into two contributions, namely the cost of self-propulsion and an additional amount of dissipation which arises from spin-spin interaction that is responsible for alignment. The flocking phase emerges when the spin-spin alignment strength is increased above a critical value. As the alignment strength increases, the dissipation of self-propulsion stays constant while the alignment dissipation reaches its maximum exactly at the flocking transition point with a cusp singularity (divergent second derivative) in the thermodynamic limit (fixed density and infinite volume). To understand these results, we analytically solve a reduced AIM with only two sites. The two-site model can be considered a coarse-grained version of the AIM and it captures the essential behaviors of the energy dissipation, most notably the cusped maximum at the flocking transition. Our study reveals an energy-speed-sensitivity trade-off in flocking, which relates the dissipation rate of the system to the speed and sensitivity of the flocking phase. The state-space probability flux is also investigated in the flocking and non-flocking phases, which suggests a possible analogy to phase transition in a system of interacting dipoles.

Dissipation in the active Ising model (AIM). The 2D AIM describes N particles on a $L_x \times L_y$ lattice with periodic boundary conditions. Each particle carries an Ising spin $s = \pm 1$, and the number of $\pm$ spins on site (i, j) is denoted by $n^{\pm}_{i,j}$ (no volume exclusion). The system follows continuous-time Markovian dynamics including flipping (local alignment) and hopping (self-propulsion). Each particle can flip its spin from s to $(-s)$ at rate $\omega e^{-\beta E_0 s m_{i,j}/\rho_{i,j}}$, where $m_{i,j} = n^+_{i,j} - n^-_{i,j}$ and $\rho_{i,j} = n^+_{i,j} + n^-_{i,j}$ are the local magnetization and density, respectively. ω^{-1} sets the flipping timescale. E_0 measures the strength of the spin-spin alignment interaction, and β is the inverse temperature which is set to 1. Each spin can also hop to one of the four neighboring sites, at rate $D(1 + s\epsilon)$ to the right, $D(1 - s\epsilon)$ to the left, and D to up and down. The flipping dynamics obeys detailed balance according to the Hamiltonian of a fully-

connected (mean-field) Ising model, but the hopping dynamics breaks detailed balance and drives the system out of equilibrium. With $\epsilon \neq 0$ and large enough E_0 and/or ρ, the system exhibits collective flocking behavior [11, 12], as characterized by a nonzero mean flocking speed (order parameter) $v = 2D\epsilon \langle s \rangle$ in the x-direction.

Two equivalent approaches are employed to calculate the steady-state entropy production (energy dissipation) rate. In the first method, the average dissipation rate is calculated from the ratio of forward and backward realizations of a sufficiently long trajectory (assuming ergodicity) obtained by simulating the AIM dynamics [30]. The second approach considers the different spin configurations ($\{n^{\pm}_{i,j}\}$) as states of a reaction network with flipping and hopping as the two types of transitions between different states. Once the AIM reaction network reaches its nonequilibrium state state (NESS), the dissipation rate can be determined by following the standard procedure for computing entropy production rate of reaction networks [31, 32]. These two approaches are equivalent. The former is suited for the numerical simulation of the full AIM, and the latter is used to analytically solve the two-site AIM for mechanistic interpretation.

A finite amount of energy dissipation is needed to drive the system sufficiently away from equilibrium to generate flocking behavior. As shown in Fig. 1A, a nonzero flocking speed v can be achieved by increasing ϵ at fixed E_0, which also increases the total dissipation rate $\dot{W}_{\rm tot}$. The flocking motion does not emerge until $\dot{W}_{\rm tot}$ is above a certain (nonzero) threshold.

The total dissipation rate can be decomposed into contributions from the two types of transitions: $\dot{W}_{\rm tot} = \dot{W}_m + \dot{W}_a$, where $\dot{W}_m$ and $\dot{W}_a$ correspond to the dissipation rates due to motion (hopping) and alignment (flipping) of the particles, respectively. Since each particle moves at an average speed $v_0 = 2D\epsilon$ and each step along the bias direction costs energy $\ln \frac{1+\epsilon}{1-\epsilon}$, the resulting dissipation rate for motion is simply $\dot{W}_m = N v_0 \ln \frac{1+\epsilon}{1-\epsilon}$. The alignment dissipation $\dot{W}_a$ can be calculated by summing up the cost of all flipping events during a sufficiently long time interval τ (after the system reaches steady-state):

$$\dot{W}_a = \lim_{\tau\to\infty} \frac{1}{\tau} \sum_{0<t<\tau} 2E_0 \frac{1 - m_{i,j} s}{\rho_{i,j}}. \qquad (1)$$

Each event flips a spin s to $(-s)$ on site (i, j), which has local magnetization $m_{i,j}$ and local density $\rho_{i,j}$ (see Supplementary Information (SI) for details). It will be convenient to henceforth refer to the nondimensionalized alignment dissipation rate $\dot{w}_a = \dot{W}_a/(2\omega E_0)$ as the alignment dissipation.

The motion dissipation rate $\dot{W}_m$ is responsible for driving the self-propulsion of the particles, which is independent of the alignment dynamics. As expected, $\dot{W}_m$ vanishes for the equilibrium Brownian motion without bias ($\epsilon = 0$) and increases with the bias ϵ. For the extreme case $\epsilon \to 1$, the hopping motion is irreversible and $\dot{W}_m \to \infty$. The origin of the alignment dissipation $\dot{W}_a$ is more subtle. Although the local spin flipping dynamics obeys detailed balance, the local spin system at a given site is driven out of equilibrium by the continuous injection and ejection of new spins from its neighboring sites due to the transport process and a continuous dissipation rate $\dot{W}_a$ is needed to drive the spin alignment to maintain the flocking order. As a result, $\dot{W}_a$ depends on both the alignment strength (E_0) and the particle's key transport properties in particular the motion bias ϵ and the relative timescale D/ω. Next, we investigate how the flocking behavior and dissipation rates depend on the these key control parameters of the system (E_0, ϵ, D/ω), from which we aim to uncover possible cost-performance relationship of the flocking behavior.

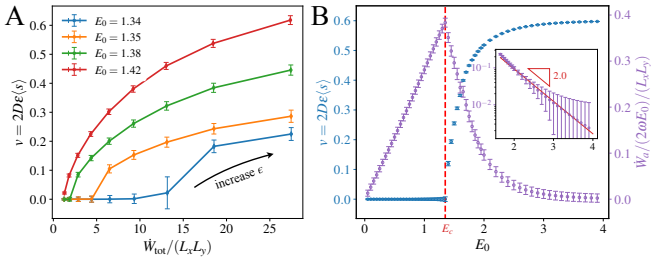

FIG. 1. (A) The average flocking speed v versus the total dissipation $\dot{W}_{\rm tot}$ for fixed values of E_0 and increasing ϵ. (B) The average flocking speed (blue) and alignment dissipation (purple) for $\epsilon = 0.3$. The red dashed line is the transition point E_c above which $v > 0$. The inset shows the exponential decay of dissipation at large E_0. $L_x = 300$, $L_y = 100$, $\bar{\rho} = N/(L_xL_y) = 5$, $D = 1$, $\omega = 1$.

A cusped dissipation maximum at the flocking transition. For a fixed bias ϵ, the system remains disordered ($v = 0$) until E_0 is increased above a certain threshold E_c (Fig. 1B). The alignment dissipation $\dot{w}_a$ increases linearly in the disordered phase and decreases monotonically in the flocking phase (exponentially at large E_0 as shown by the inset). Remarkably, it reaches maximum exactly at the transition point E_c in the form of a cusp. The value of $\dot{w}_a$ is continuous across the transition, but its derivative $\frac{{\rm d}\dot{w}_a}{{\rm d}E_0}$ changes abruptly from positive to negative across E_c forming a cusp at its maximum. Since $\dot{W}_m$ stays constant, the same cusped maximum behavior also exists for $\dot{W}_{\rm tot}$. Extensive numerical simulations find this behavior to be general, regardless of the bias ϵ or the relative timescale set by D/ω (see SI). The critical E_c decreases with ϵ and increase with ω, but it always coincides with the maximum of $\dot{w}_a$. The alignment dissipation can be decomposed into the product of the frequency of flipping events $\dot{n}_f$ and the mean energy cost per flip $\bar{w}_f = \dot{w}_a/\dot{n}_f$. At the transition point, they both have continuous values but discontinuous first derivatives, which results in the cusp of $\dot{w}_a$ (see SI).

As discussed previously, the key to understanding

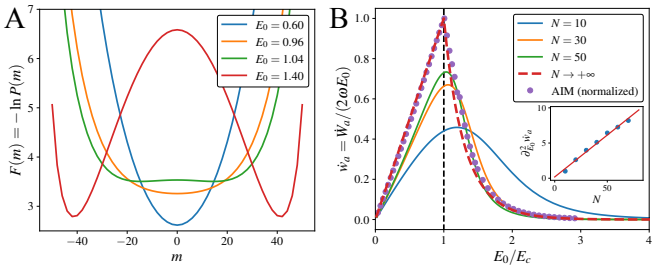

FIG. 2. (A) The effective free energy landscape demonstrates the existence of a nonequilibrium phase transition. $N = 50$, $D = \omega = 1$. (B) The alignment dissipation: solid lines, two-site AIM with different finite N; dashed line, the infinite N solution of the two-site AIM; dots, the full AIM ($L_x = 300$, $L_y = 100$). The full AIM curve has been normalized in the x direction by the critical E_c and in the y direction by its maximum. The inset shows that the curvature at the two-site dissipation maximum diverges with N, leading to a cusp at infinite N.

the alignment dissipation is how the transport of spins from/to neighboring sites drives the local spin system out of equilibrium. However, it is difficult to understand the full AIM with a large system size due to the numerous degrees of freedom. Next, we investigate the alignment dissipation in a reduced AIM with the minimal number of sites that allows transport of active spins.

The two-site AIM shows the cusped maximum of flocking dissipation. We consider a special case of the AIM with only two sites ($L_x = 2$ and $L_y = 1$), which is the minimum system size needed to drive the AIM out of equilibrium to produce flocking behavior. Conceptually, the two-site AIM can be considered as the result of iterative coarse-graining of the full AIM following the real space renormalization group approach [33, 34] until only two sites remain.

The model is fully characterized by the total number of spins N and three state variables (a_0, a_1, b_1) where a_0 is the total number of $+$ spins; a_1 and b_1 correspond to the number of $+$ and $-$ spins on site 1, respectively. The dynamics of the probability distribution $P(a_0, a_1, b_1)$ is governed by the master equation:

$$\frac{\mathrm{d}P(a_0, a_1, b_1)}{\mathrm{d}t} = \mathcal{L}P(a_0, a_1, b_1), \tag{2}$$

where $\mathcal{L}$ is a linear operator capturing the transitions, which can be expressed as a $N^3 \times N^3$ matrix (see SI for details). The steady-state distribution $P^s(a_0, a_1, b_1)$ can be found by solving $\mathcal{L}P^s(a_0, a_1, b_1) = 0$ subject to normalization $\sum_{a_0,a_1,b_1} P^s(a_0, a_1, b_1) = 1$, and can be used to compute all statistical properties of the system, e.g., the average total magnetization $\langle m\rangle = \sum_{a_0,a_1,b_1}(2a_0 - N)P^s(a_0, a_1, b_1)$.

For a finite N, the phase transition point E_c can be determined by computing the effective free energy landscape $F(m) = -\ln P(m)$ where $P(m) = \sum_{a_0,a_1,b_1} \delta(2a_0 - N - m)P^s(a_0, a_1, b_1)$ is the steady-state distribution of the total magnetization m. As shown in Fig. 3A, as E_0 increases, the disordered state $m = 0$ goes from stable ($F''(0) > 0$) to unstable ($F''(0) < 0$), which indicates the emergence of flocking. The difference between the transition point E_c (determined from $F''(0) = 0$) and the position of the alignment dissipation maximum ($E_m = \arg\max_{E_0} \dot{w}_a$) vanishes with at infinite N (see SI), consistent with the dissipation maximum at flocking transition found in the full AIM. Moreover, the curvature at the peak $\partial^2_{E_0}\dot{w}_{\mathrm{flip}}\big|_{E_0=E_m}$ increases with N (Fig. 3B inset) and it is projected to diverge in the infinite N limit, which is consistent with the cusped dissipation maximum observed in the full AIM.

In the infinite N limit, the steady-state probability P^s can be obtained analytically by assuming time scale separation $D \gg \omega$. The assumption is not essential to the results (see SI for numerical evidence), but it enables factorization of the probability distribution P^s

$$P^s(a_0, a_1, b_1) = P(m)\binom{a_0}{a_1}\binom{N - a_0}{b_1}, \tag{3}$$

to analytically obtain the effective free energy landscape:

$$\frac{F(m)}{N} = z\ln z + (1-z)\ln(1-z) + 2E_0 z(1-z) + O(N^{-1}) \tag{4}$$

where $z = a_0/N = (N + m)/(2N)$ is the fraction of spin up (see SI for derivation). The flocking transition takes place at $E_c = 1$, where the most probable state (saddle point) goes from the disordered state ($z = \frac{1}{2}$) to the flocking state with $z = z^\star(\neq \frac{1}{2})$ where $z^\star$ is determined by

$$\frac{1}{2(1-2z^\star)}\ln\frac{1-z^\star}{z^\star} = E_0, \quad (E_0 > 1) \tag{5}$$

which has two solutions $z^\star$ and $(1 - z^\star)$ corresponding to flocking leftwards and rightwards, respectively. Although the free energy is equivalent to that of the mean-field Ising model, the system continuously dissipates energy due to non-vanishing state-space fluxes. The fluxes associated with flipping give the alignment dissipation $\dot{w}_a$:

$$\dot{w}_a = \frac{1}{2\omega E_0}\sum_{\mathrm{flip}}(J_+ - J_-)\ln\frac{J_+}{J_-} = N\langle w_1\rangle + \langle w_0\rangle + O\big(N^{-1}\big), \tag{6}$$

where $w_{0,1}$ are functions of (a_0, a_1, b_1) and parameters, and $\langle w\rangle = \sum wP^s$ means averaging over the steady-state probability distribution, which can be calculated using the saddle-point method. Importantly, the mean-field Ising P^s will cause any direct evaluation of dissipation at the saddle point to vanish. The leading order contribution comes from expanding w near the saddle point to the second order, which leads to $\langle w_{0,1}\rangle \sim O(N^{-1})$. Therefore, the dominating term in $\dot{w}_a$ comes from expanding

w_1 near the saddle point:

$$\dot{w}_a = \frac{N}{2}\left[\frac{\partial^2 w_1}{\partial a_1^2}\left\langle (a_1 - a_1^\star)^2\right\rangle + \frac{\partial^2 w_1}{\partial b_1^2}\left\langle (b_1 - b_1^\star)^2\right\rangle\right] = \begin{cases} E_0, & 0 < E_0 < E_c (= 1) \\ 8E_0[z^\star(1-z^\star)]^{3/2}, & E_0 \geq E_c \end{cases}, \tag{7}$$

where both derivatives are evaluated at the saddle point $(a_0^\star, a_1^\star, b_1^\star) = (z^\star N, z^\star N/2, (1-z^\star)N/2)$. It is clear from Eq. 7 that $\partial_{E_0}\dot{w}_a$ is discontinuous at the critical point ($E_0 = E_c$) because $\partial_{E_0} z^\star$ is discontinuous there. Quantitatively, we have $\partial_{E_0}\dot{w}_a|_{E_0=1^-} = 1$ and $\partial_{E_0}\dot{w}_a|_{E_0=1^+} = -3.5$, which shows that $\dot{w}_a$ (red dashed line in Fig. 2B) exhibits a cusped maximum exactly at $E_c = 1$. It is also interesting to note from Eq. 7 that the alignment energy cost $\dot{w}_a$ depends on variance of the local spin number fluctuations ($\langle (a_1 - a_1^\star)^2\rangle$ and $\langle (b_1 - b_1^\star)^2\rangle$), which are driven by the transport process.

To make a direct comparison between the two-site AIM and the full AIM, we rescale E_0 by E_c, normalize the dissipation by its maximum, and plot them against each other in Fig. 2B. The two models agree exactly in the disordered phase where dissipation grows linearly with E_0 as well as deep in the flocking phase where dissipation decays exponentially to zero. The cusped maximum at transition is also in good agreement, evident from the discontinuity of the slope. The small difference at E_0 slightly above E_c can be explained by the difference in the order of the phase transition. The first-order transition found in the full AIM becomes second-order in the two-site AIM, which can be understood from the RG perspective where coarse-graining eliminates phase-coexistence by washing out the phase with the smaller volume fraction.

One hallmark of nonequilibrium systems is the existence of steady-state divergence-free probability fluxes (cycles) in state space, which play a central role in nonequilibrium information processing such as adaptation [14] and proofreading [15, 20, 35]. These persistent fluxes are also the origin of steady-state energy dissipation [31, 32, 36, 37]. Here, we consider how the fluxes are related to the flocking order and the energy dissipation. Fig. 3A&B show the flocking dissipation density and the fluxes in the $(m, \Delta\rho)$ plane in the non-flocking and flocking phases, respectively, where $\Delta\rho = 2(a_1 + b_1) - N$ is the density difference between the two sites. In both phases, the dissipation comes from the uniform configuration near $\Delta\rho \sim 0$. The dissipation is concentrated around $m = 0$ in the non-flocking phase and at large $|m|$ in the flocking phase. The divergence-free fluxes form vortices related to each other by symmetries (between the two sites and between spin up and down). In the non-flocking phase, there are four vortices that form a tight quadrupole, which can be considered as a bound pair of anti-parallel dipoles (see inset in Fig. 3A). In the flocking phase, the quadrupole splits into two dipoles separated in the m direction, each accompanied by a smaller anti-parallel dipole (see inset in Fig. 3B). The flocking transition is thus analogous to the unbinding of a pair of dipoles. Both confined and free dipoles lead to low dissipation, but high dissipation occurs during the transition. This analogy is reminiscent of the mapping between the Kosterlitz-Thouless phase transition and the Coulomb gas [38–40], where the binding/unbinding of topological defects can be mapped to those of Coulomb charges. Here, the charges always appear in dipoles as active spins visit the two sites alternatively. Therefore, we speculate that the analogy could be the confinement/release of interacting dipoles with their interactions governed by alignment strength (E_0) and motion bias (ϵ).

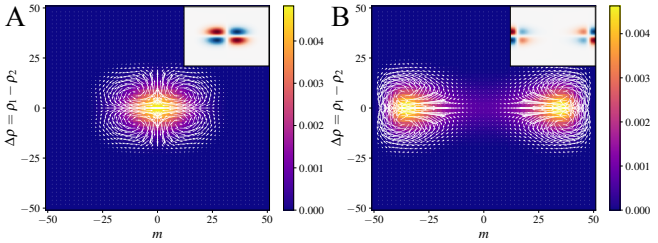

FIG. 3. The alignment dissipation density (heatmaps) and probability fluxes (white arrows) of the two-site model in (A) non-flocking phase ($E_0 = 0.6$) and (B) flocking phase ($E_0 = 1.4$). The insets show vorticity of probability fluxes. $N = 50$, $D = \omega = 1$.

The energy-speed-sensitivity trade-off. The flocking of interacting particles is conceptually analogous to the synchronization of coupled oscillators [41, 42], which can be understood as flocking in the state (phase of the clock) space. In both cases, an extra energy dissipation is needed to maintain coherence among individual subsystems (spins/oscillators) that are already out of equilibrium. However, the dissipation of these two systems exhibits different behaviors. For coupled oscillators, the dissipation increases with the order parameter, meaning that it is very costly to maintain a system of highly coupled (and therefore synchronized) oscillators [42]. In the AIM, however, dissipation peaks exactly at the transition and decreases with interaction (E_0) in the flocking phase. At large E_0, the highly ordered flock requires a smaller energy to maintain. The difference between the two behaviors stems from the alignment mechanisms. The active spins align locally, which effectively synchronizes their velocities. The coupled oscillators are synchronized by exchanging phases, which corresponds to simultaneously displacing pairs of particles in the AIM. This non-local interaction couples the alignment cost to the cost of motion (i.e. advancing the individual clocks), leading to a higher dissipation in the ordered phase. These analyses suggest that compared to exchanging position, local alignment of velocity is an energetically more favorable way of maintaining the order in a system of active

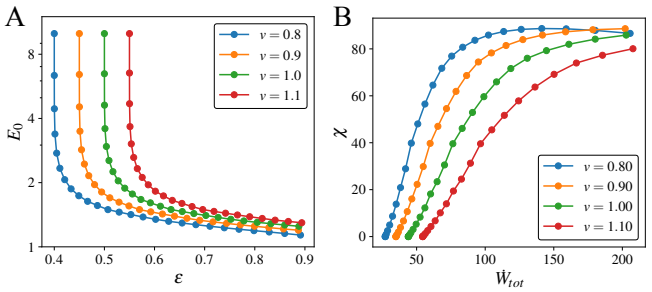

FIG. 4. The energy-speed-sensitivity trade-off in the two-site AIM. (A) Contours for constant v in the (ϵ, E_0) plane. (B) The total dissipation and sensitivity along different v contours. $N = 40$, $D = \omega = 1$.

particles.

It may seem surprising that natural flocks do not always reside in the strong interaction (large E_0) regime which offers the benefits of both higher ordering and lower dissipation. Starling flocks, for example, are suggested to behave like critical systems [43]. A potential explanation is the need for high sensitivity, which increases as the system approaches its flocking transition. We characterize sensitivity by the magnetic susceptibility χ of the AIM. In AIM, there are many choices of parameters (ϵ, E_0) to achieve any given flocking speed v as shown in Fig. 4A. For a given v, the total dissipation is at its minimum in the limit of $E_0 \to \infty$ and $\epsilon \to v/(2D)$. However, this minimum cost system at $E_0 = \infty$ has zero sensitivity ($\chi = 0$). In general, sensitivity can be increased by decreasing E_0, which requires increasing ϵ in order to maintain a fixed v (Fig. 4A). As a result, $\dot{W}_m$ and thereby the total dissipation increases. Fig. 4B demonstrates this trade-off whereby enhancing sensitivity at a constant flocking speed necessarily increases dissipation. Similarly, for a given sensitivity, increasing the flocking speed also requires more dissipation; for a given dissipation, increasing speed leads to decrease of sensitivity (see SI for analytical expressions). These relations constitute an energy-speed-sensitivity trade-off, which places natural flocks at some intermediate regime that maximizes the overall fitness.

Discussion and future directions. It is quite remarkable that highly nontrivial characteristics of the dissipation profile such as the cusped maximum at the critical point can be captured and explained by the simple two-site AIM. Given that the two-site AIM can be considered as a coarse-grained version of the full AIM, it will be interesting to investigate what is the appropriate coarse-graining procedure that preserves the dissipation characteristics in particular the cusped maximum behavior, and whether there is scaling law for the dissipation as suggested by recent studies of general reaction networks [27–29]. Another possible direction to explore is to extend this study to flocking theories with continuous symmetry and off-lattice models [6–8]. Finally, the energy-speed-sensitivity trade-off uncovered in this study may provide a useful perspective for understanding dynamics of natural flocks and designing optimal control of artificial flocks.

This work is supported in part by National Institutes of Health grant R35GM131734 (to Y. T.). Q. Y. thanks Luca Di Carlo, Dongliang Zhang, Qi Ouyang, and Chao Tang for helpful discussions.

[1] J. Toner, Y. Tu, and S. Ramaswamy, Hydrodynamics and phases of flocks, Annals of Physics **318**, 170 (2005).
[2] S. Ramaswamy, The Mechanics and Statistics of Active Matter, Annual Review of Condensed Matter Physics **1**, 323 (2010).
[3] M. C. Marchetti, J. F. Joanny, S. Ramaswamy, T. B. Liverpool, J. Prost, M. Rao, and R. A. Simha, Hydrodynamics of soft active matter, Rev. Mod. Phys. **85**, 1143 (2013).
[4] W. Bialek, A. Cavagna, I. Giardina, T. Mora, E. Silvestri, M. Viale, and A. M. Walczak, Statistical mechanics for natural flocks of birds, Proc. Natl. Acad. Sci. U.S.A. **109**, 4786 (2012).
[5] A. Kaiser, A. Snezhko, and I. S. Aranson, Flocking ferromagnetic colloids, Sci. Adv. **3**, e1601469 (2017).
[6] T. Vicsek, A. Czirók, E. Ben-Jacob, I. Cohen, and O. Shochet, Novel type of phase transition in a system of self-driven particles, Phys. Rev. Lett. **75**, 1226 (1995).
[7] J. Toner and Y. Tu, Long-Range Order in a Two-Dimensional Dynamical XY Model: How Birds Fly Together, Phys. Rev. Lett. **75**, 4326 (1995).
[8] J. Toner and Y. Tu, Flocks, herds, and schools: A quantitative theory of flocking, Phys. Rev. E **58**, 4828 (1998).
[9] G. Grégoire and H. Chaté, Onset of Collective and Cohesive Motion, Phys. Rev. Lett. **92**, 025702 (2004).
[10] H. Chaté, F. Ginelli, G. Grégoire, and F. Raynaud, Collective motion of self-propelled particles interacting without cohesion, Phys. Rev. E **77**, 046113 (2008).
[11] A. P. Solon and J. Tailleur, Revisiting the Flocking Transition Using Active Spins, Phys. Rev. Lett. **111**, 078101 (2013).
[12] A. P. Solon and J. Tailleur, Flocking with discrete symmetry: The two-dimensional active Ising model, Phys. Rev. E **92**, 042119 (2015).
[13] F. S. Gnesotto, F. Mura, J. Gladrow, and C. P. Broedersz, Broken detailed balance and non-equilibrium dynamics in living systems: a review, Rep. Prog. Phys. **81**, 066601 (2018).
[14] G. Lan, P. Sartori, S. Neumann, V. Sourjik, and Y. Tu, The energy–speed–accuracy trade-off in sensory adaptation, Nature Phys **8**, 422 (2012).
[15] J. J. Hopfield, Kinetic Proofreading: A New Mechanism for Reducing Errors in Biosynthetic Processes Requiring High Specificity, Proc. Natl. Acad. Sci. U.S.A. **71**, 4135 (1974).
[16] J. Ninio, Kinetic amplification of enzyme discrimination, Biochimie **57**, 587 (1975).
[17] C. H. Bennett, Dissipation-error tradeoff in proofreading, Biosystems **11**, 85 (1979).

[18] A. Murugan, D. A. Huse, and S. Leibler, Speed, dissipation, and error in kinetic proofreading, Proc. Natl. Acad. Sci. U.S.A. **109**, 12034 (2012).

[19] P. Sartori and S. Pigolotti, Thermodynamics of Error Correction, Phys. Rev. X **5**, 041039 (2015).

[20] Q. Yu, A. B. Kolomeisky, and O. A. Igoshin, The energy cost and optimal design of networks for biological discrimination, J. R. Soc. Interface. **19**, 20210883 (2022).

[21] Y. Cao, H. Wang, Q. Ouyang, and Y. Tu, The free-energy cost of accurate biochemical oscillations, Nature Phys **11**, 772 (2015).

[22] H. Chaté, Dry Aligning Dilute Active Matter, Annual Review of Condensed Matter Physics **11**, 189 (2020).

[23] U. Seifert, Stochastic thermodynamics, fluctuation theorems and molecular machines, Rep. Prog. Phys. **75**, 126001 (2012).

[24] C. Nardini, É. Fodor, E. Tjhung, F. van Wijland, J. Tailleur, and M. E. Cates, Entropy Production in Field Theories without Time-Reversal Symmetry: Quantifying the Non-Equilibrium Character of Active Matter, Phys. Rev. X **7**, 021007 (2017).

[25] É. Fodor, R. L. Jack, and M. E. Cates, Irreversibility and Biased Ensembles in Active Matter: Insights from Stochastic Thermodynamics, Annual Review of Condensed Matter Physics **13**, 215 (2022).

[26] T. Markovich, É. Fodor, E. Tjhung, and M. E. Cates, Thermodynamics of Active Field Theories: Energetic Cost of Coupling to Reservoirs, Phys. Rev. X **11**, 021057 (2021).

[27] Q. Yu, D. Zhang, and Y. Tu, Inverse Power Law Scaling of Energy Dissipation Rate in Nonequilibrium Reaction Networks, Phys. Rev. Lett. **126**, 080601 (2021).

[28] Q. Yu and Y. Tu, State-space renormalization group theory of nonequilibrium reaction networks: Exact solutions for hypercubic lattices in arbitrary dimensions, Phys. Rev. E **105**, 044140 (2022).

[29] L. Cocconi, G. Salbreux, and G. Pruessner, Scaling of entropy production under coarse graining in active disordered media, Phys. Rev. E **105**, L042601 (2022).

[30] L. Peliti and S. Pigolotti, *Stochastic thermodynamics: an introduction* (Princeton University Press, Princeton, 2021).

[31] T. L. Hill, *Free energy transduction in biology: the steady-state kinetic and thermodynamic formalism* (Academic Press, New York, 1977).

[32] H. Qian, Open-System Nonequilibrium Steady State: Statistical Thermodynamics, Fluctuations, and Chemical Oscillations, J. Phys. Chem. B **110**, 15063 (2006).

[33] L. P. Kadanoff, Scaling laws for ising models near T c, Physics Physique Fizika **2**, 263 (1966).

[34] K. G. Wilson, The renormalization group: Critical phenomena and the Kondo problem, Rev. Mod. Phys. **47**, 773 (1975).

[35] M. A. Savageau and D. S. Lapointe, Optimization of kinetic proofreading: A general method for derivation of the constraint relations and an exploration of a specific case, Journal of Theoretical Biology **93**, 157 (1981).

[36] J. Schnakenberg, Network theory of microscopic and macroscopic behavior of master equation systems, Rev. Mod. Phys. **48**, 571 (1976).

[37] R. K. P. Zia and B. Schmittmann, Probability currents as principal characteristics in the statistical mechanics of non-equilibrium steady states, J. Stat. Mech. Theory Exp. **2007**, P07012 (2007).

[38] V. Berezinskii, Destruction of long-range order in one-dimensional and two-dimensional systems possessing a continuous symmetry group. ii. quantum systems, Sov. Phys. JETP **34**, 610 (1972).

[39] J. M. Kosterlitz and D. J. Thouless, Ordering, metastability and phase transitions in two-dimensional systems, J. Phys. C: Solid State Phys. **6**, 1181 (1973).

[40] J. M. Kosterlitz, The critical properties of the two-dimensional xy model, J. Phys. C: Solid State Phys. **7**, 1046 (1974).

[41] Y. Kuramoto, *Chemical oscillations, waves, and turbulence* (Courier Corporation, 2003).

[42] D. Zhang, Y. Cao, Q. Ouyang, and Y. Tu, The energy cost and optimal design for synchronization of coupled molecular oscillators, Nat. Phys. **16**, 95 (2020).

[43] A. Cavagna, A. Cimarelli, I. Giardina, G. Parisi, R. Santagati, F. Stefanini, and M. Viale, Scale-free correlations in starling flocks, Proc. Natl. Acad. Sci. U.S.A. **107**, 11865 (2010).